

Article

# Dual-Circularly Polarized 60 GHz Beam-Steerable Antenna Array with $8 \times 8$ Butler Matrix

Yuntae Park, Jihoon Bang and Jaehoon Choi \* 

Department of Electronics and Computer Engineering, Hanyang University, Seoul 04763, Korea; yuntae1101@hanyang.ac.kr (Y.P.); bangjh@hanyang.ac.kr (J.B.)

\* Correspondence: choijh@hanyang.ac.kr; Tel.: +82-2-2220-0376

Received: 2 January 2020; Accepted: 27 March 2020; Published: 1 April 2020



**Abstract:** A beam-steerable dual-circularly polarized 60 GHz antenna array is proposed. A  $1 \times 4$  dual-fed stacked patch antenna array is integrated with an  $8 \times 8$  Butler matrix. By utilizing the  $8 \times 8$  Butler matrix, the proposed antenna array generates dual-circular polarization with beam-steering capability. The proposed antenna array system demonstrates good reflection coefficients in the frequency band ranging from 55.3 GHz to 64.9 GHz and has a mutual coupling of less than  $-10$  dB over the frequency range of 57.5 GHz–63.2 GHz. At 60 GHz, the maximum gains and beam-steering angles for input ports 2, 4, 5, and 7 are 9.39 dBi at  $-38^\circ$ , 10.67 dBi at  $-11^\circ$ , 10.63 dBi at  $+11^\circ$ , and 9.38 dBi at  $+39^\circ$ , respectively. It is also demonstrated that the dual-polarization is well formed by switching the excitation ports. The right-handed circular polarization (RHCP) is formed when four ports from port 1 to port 4 are excited and left-handed circular polarization (LHCP) is formed when four ports from port 5 to port 8 are excited. The proposed antenna array system could be a good candidate for millimeter-wave 5G applications that require wide beam coverage and polarization diversity.

**Keywords:** beam-steering; dual-polarization; circular polarization; antenna array; Butler matrix; right-handed circular polarization (RHCP); left-handed circular polarization (LHCP); 60 GHz; 5G

## 1. Introduction

Recently, various studies on millimeter-wave communication technologies have been performed to provide higher data rates and increased system capacities. 60 GHz-based millimeter-wave communication is attractive for a number of reasons, including a large amount of spectrum availability, miniaturization capability, superior frequency reuse, and a multi-gigabit data rate. In the millimeter-wave frequency bands, due to atmospheric absorption, the free-space path loss is more significant than that in conventional cellular bands below 6 GHz. To compensate for the high path loss over millimeter-wave frequencies, array antennas with high gain are commonly used. Since array antennas have a directional beam pattern with limited beam coverage, it should be designed to have beam-steering capability with the proper beam pattern to obtain a wide communication coverage [1], [2]. Among the various beam-steering techniques, switched beam networks have been highlighted because of the advantages of low cost, simple implementation, and low power consumption. The Butler matrix is one of the switched beam networks and is especially popular due to its simpler structure and wider bandwidth [3–12].

Meanwhile, polarization diversity and the use of circular polarization are important to improve the spectral efficiency and compensate for the polarization mismatch in wireless communication systems. In particular, the use of circular polarization can effectively suppress multi-path fading in line-of-sight (LOS) environments and give a higher probability of a successful link [13–18]. This is due to the fact that circularly polarized signals are much better at penetrating and bending around obstacles compared with linearly polarized signals.

Several research works have been reported in designing the phased array antenna using the Butler matrix for millimeter-wave applications. However, most of previous research only dealt with improvement of the Butler matrix performances, such as an isolation between the ports and an amplitude imbalance at the output ports. On the other hand, only a few studies focused on not only those performances but also on their polarization properties. In [19], circular polarization was achieved by using a  $1 \times 6$  magneto-electric dipole antenna array with a  $5 \times 6$  Butler matrix. In [20], the polarization diversity was considered together with the dual-polarization characteristic using a waveguide-type Butler matrix.

In this paper, we propose a dual-circularly polarized 60 GHz beam-steerable patch antenna array with an  $8 \times 8$  Butler matrix to simultaneously resolve the limited beam coverage and polarization mismatch in millimeter-wave wireless communication systems.

## 2. Design of Antenna Array System

The block diagram of the designed switching beamforming antenna array system is illustrated in Figure 1. The designed switching beamforming network is implemented based on a Butler matrix, and the antenna array is implemented using patch elements. The Butler matrix generates output signals with different phases and feeds the antenna array, which enables the beam-steering of the antenna in different directions.

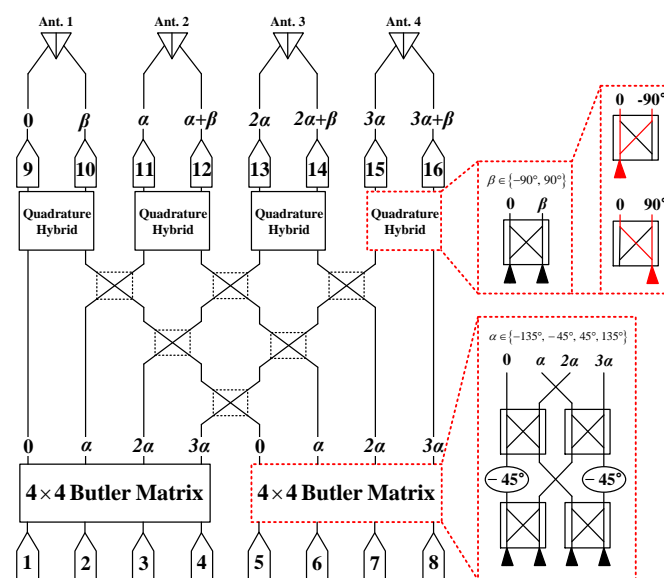


Figure 1. Block diagram of the switched-beam network.

Figure 2 shows the configuration of the proposed antenna array system. The antenna array system is fabricated on a three-layer Taconic TLY substrate with a relative permittivity of 2.2, a loss tangent of 0.0009, and a thickness of 0.254 mm. The proposed antenna array system mainly consists of three parts, which include an  $8 \times 8$  Butler matrix, a transition, and a stacked patch antenna array.

The structure of the  $8 \times 8$  Butler matrix is shown in Figure 3. The  $8 \times 8$  Butler matrix, which is based on the design scheme suggested in [3], consists of two  $4 \times 4$  Butler matrices and additional parts to obtain the desired output phase distribution, as listed in Table 1. Each Butler matrix and the additional parts consist of stripline-based quadrature hybrid couplers, crossovers, and phase-balancing dummy crossovers. The line width of the striplines in the Butler matrix design are set to 0.17 mm to obtain a  $50 \Omega$  characteristic impedance.

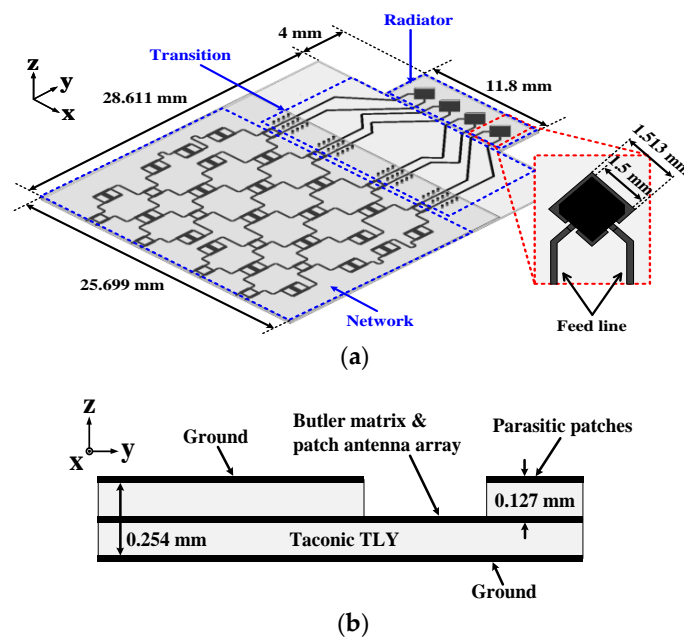


Figure 2. Configuration of the proposed antenna array system: (a) 3D-view and (b) side-view.

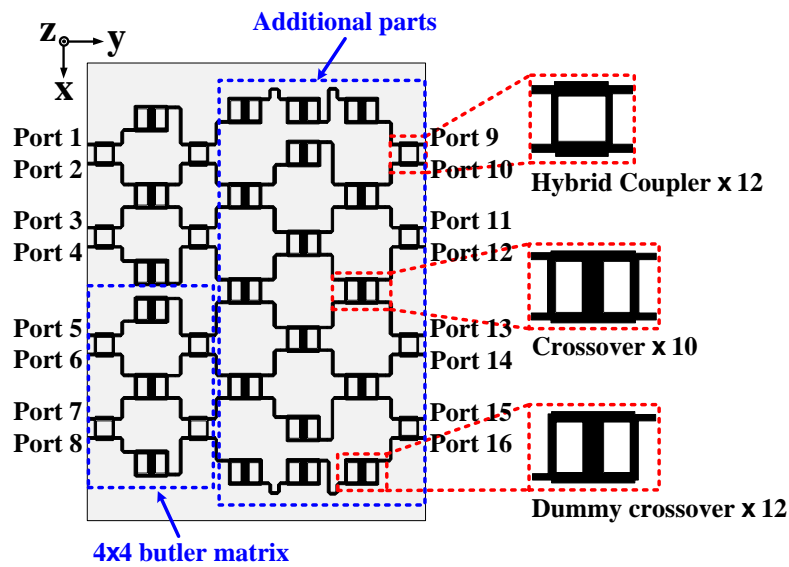


Figure 3. Structure of the 8 × 8 Butler matrix.

Table 1. Phases associated with the selected port of the 8 × 8 Butler matrix.

	Output Phase [Degree]							
	Port 9	Port 10	Port 11	Port 12	Port 13	Port 14	Port 15	Port 16
Port 1	0°	−90°	−45°	−135°	−90°	−180°	−135°	135°
Port 2	0°	−90°	135°	45°	−90°	−180°	45°	−45°
Port 3	0°	−90°	−135°	135°	90°	0°	−45°	−135°
Port 4	0°	−90°	45°	−45°	90°	0°	135°	45°
Port 5	0°	90°	−45°	45°	−90°	0°	−135°	−45°
Port 6	0°	90°	135°	−135°	−90°	0°	45°	135°
Port 7	0°	90°	−135°	−45°	90°	180°	−45°	45°
Port 8	0°	90°	45°	135°	90°	180°	135°	−135°

The quadrature hybrid coupler is realized by two pairs of 50 Ω and 35.35 Ω quarter-wavelength striplines. Figure 4 illustrates the simulated S-parameters of the quadrature hybrid coupler when port 1 is excited. It can be seen that the return loss ( $S_{11}$ ) and the isolation ( $S_{41}$ ) are lower than  $-20$  dB over the frequency range of 57.32 GHz–63.71 GHz. Further, the calculated  $S_{21}$  and  $S_{31}$  are  $-3.02$  dB and  $-3.16$  dB at 60 GHz, respectively. This shows that the transmitted power is well divided between the two output ports, port 2 and port 3. The calculated output phases of  $S_{21}$  and  $S_{31}$  are  $-9.76^\circ$  and  $-99.69^\circ$  at 60 GHz, respectively, with a phase difference of  $89.93^\circ$ . These results agree with the theoretical scattering matrix as follows [21].

$$[S]_{Hybrid} = -\frac{1}{\sqrt{2}} \begin{bmatrix} 0 & j & 1 & 0 \\ j & 0 & 0 & 1 \\ 1 & 0 & 0 & j \\ 0 & 1 & j & 0 \end{bmatrix} \quad (1)$$

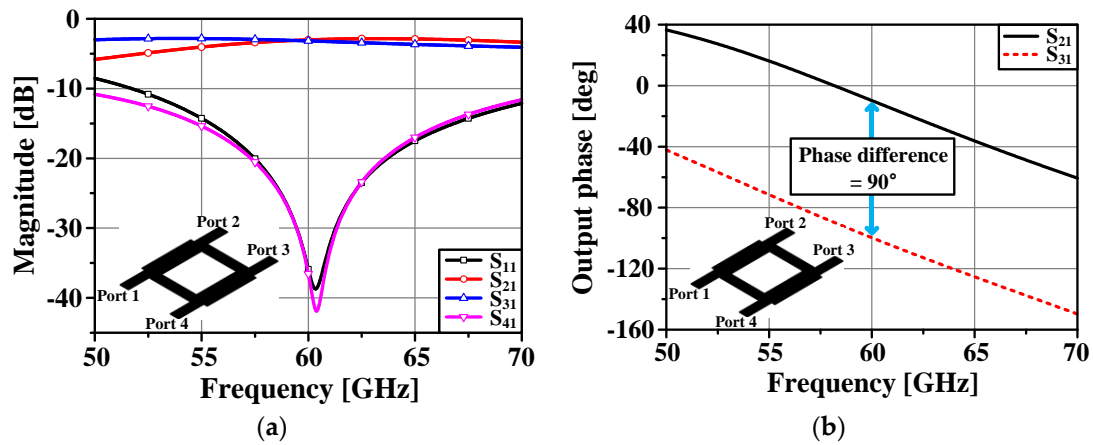


Figure 4. Simulated S-parameters of the quadrature hybrid coupler: (a) amplitude and (b) output phase.

The crossover is formed by cascading two quadrature hybrid couplers. Figure 5 shows the simulated S-parameters of the crossover when port 1 is excited. It can be seen that the return loss ( $S_{11}$ ) and isolation ( $S_{21}$  &  $S_{41}$ ) are lower than  $-15$  dB over the frequency range of 57.41 GHz–64.12 GHz. The insertion loss ( $S_{31}$ ) is calculated as  $-0.25$  dB at 60 GHz. These results coincide with the theoretical scattering matrix, as follows.

$$[S]_{Crossover} = \begin{bmatrix} 0 & 0 & j & 0 \\ 0 & 0 & 0 & j \\ j & 0 & 0 & 0 \\ 0 & j & 0 & 0 \end{bmatrix} \quad (2)$$

Note that the branch-line coupler has a high degree of symmetry so that any port can be used as an input port.

The simulated averaged insertion losses for the excitation from port 1 to port 4 of the  $8 \times 8$  Butler matrix are shown in Figure 6a, and the simulated output phases of the Butler matrix for excitation of port 4 is shown in Figure 6b. The calculated phases of  $S_{94}$ ,  $S_{10,4}$ ,  $S_{11,4}$ ,  $S_{12,4}$ ,  $S_{13,4}$ ,  $S_{14,4}$ ,  $S_{15,4}$ , and  $S_{16,4}$  are  $-117^\circ$ ,  $127^\circ$ ,  $-71^\circ$ ,  $-163^\circ$ ,  $-40^\circ$ ,  $-138^\circ$ ,  $-11^\circ$ , and  $-101^\circ$  at 60 GHz, respectively. When the phase of  $S_{94}$  is regarded as a reference ( $0^\circ$ ), the phases of ports can be written as  $0^\circ$ ,  $-116^\circ$ ,  $46^\circ$ ,  $-46^\circ$ ,  $77^\circ$ ,  $-21^\circ$ ,  $106^\circ$ , and  $16^\circ$ , respectively. On the other hand, as shown in Table 1, the desired output phases for excitation of port 4 are  $0^\circ$ ,  $-90^\circ$ ,  $45^\circ$ ,  $-45^\circ$ ,  $90^\circ$ ,  $0^\circ$ ,  $135^\circ$ , and  $45^\circ$ , respectively. The deviations between the calculated phases and desired ones for each output port are  $0^\circ$ ,  $26^\circ$ ,  $-1^\circ$ ,  $1^\circ$ ,  $13^\circ$ ,  $21^\circ$ ,  $29^\circ$ , and  $29^\circ$ , respectively. In general, the deviation below  $\pm 30^\circ$  in the Butler matrix does not significantly affect the performance of the array antenna [12].

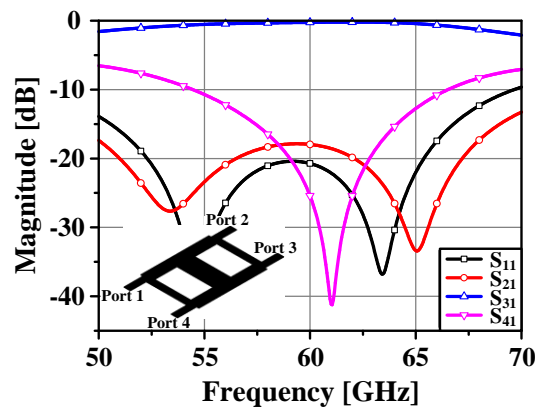


Figure 5. Simulated amplitudes of S-parameters of the crossover.

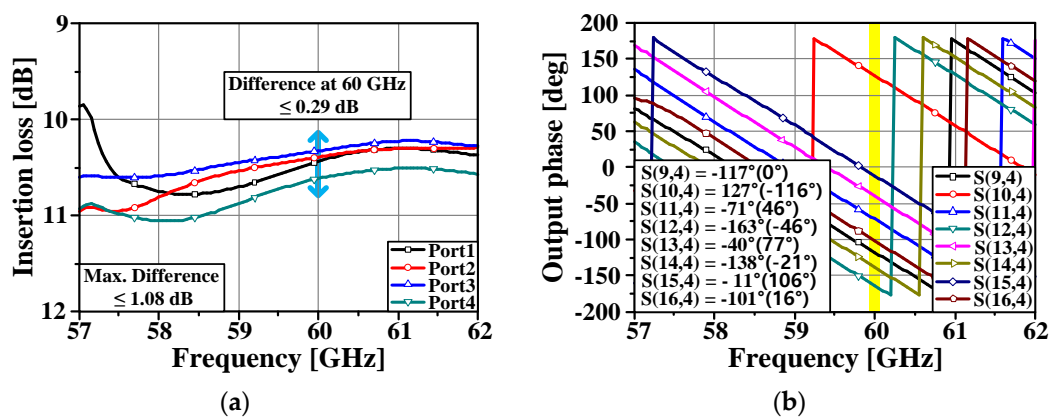


Figure 6. Simulated results of the  $8 \times 8$  Butler matrix: (a) averaged insertion losses and (b) output phase for excitation of port 4.

The configuration of the transition part to connect to the stripline-type Butler matrix with the microstrip patch antenna array is illustrated in Figure 7. The 0.17 mm widths of the stripline and microstrip line are chosen to be the same. The stripline and microstrip line share the bottom ground. The top ground of the stripline is cut out into a triangular shape at the interface between the stripline and microstrip line to obtain a good impedance matching. The series via array is also added for proper impedance matching. The radius of each via is 0.1 mm and the via array spacing is 0.5 mm. Figure 8a shows the comparison between the simulated transmission coefficients ( $S_{21}$ s) of the designed transition part with and without the via array. For the case with a series via array, unlike the case without a series via array, it can be seen that there are no resonances and large ripples on the  $S_{21}$  curves over the frequency range of 50 GHz–70 GHz. The calculated characteristic impedances of the stripline and microstrip line are  $50 \Omega$  and  $73 \Omega$ , respectively, as shown in Figure 8b.

Figure 9 shows the geometry of the designed  $1 \times 4$  patch antenna array. The proposed antenna array has four inset-fed stacked patch antenna elements with wideband characteristics. The antenna elements are designed on two stacked substrates with three layers. Each substrate has a thickness of 0.127 mm. The ground plane of the designed antenna element is on the bottom layer and the square patch and the parasitic stacked patch are positioned on the mid layer and top layer, respectively. The optimized lengths of each square patch and parasitic stacked patch are obtained as 1.513 mm and 1.5 mm, respectively. The simulated reflection coefficients for the various lengths of the parasitic stacked patch are shown in Figure 10a. The characteristic impedance of the antenna is set as  $73 \Omega$  to integrate with the designed Butler matrix. Each antenna element has two feed lines to generate the circularly polarized radiation pattern. The edges of the parasitic stacked patches are slightly cut to further guarantee that the radiation has a circular polarization. The distance between the two adjacent

elements in the designed array is 2.6 mm, which is about a half-wavelength at 60 GHz. Figure 10b shows the simulated gain pattern of the  $1 \times 4$  patch antenna array in the  $xz$ -plane at 60 GHz with the same phase and amplitude excitation.

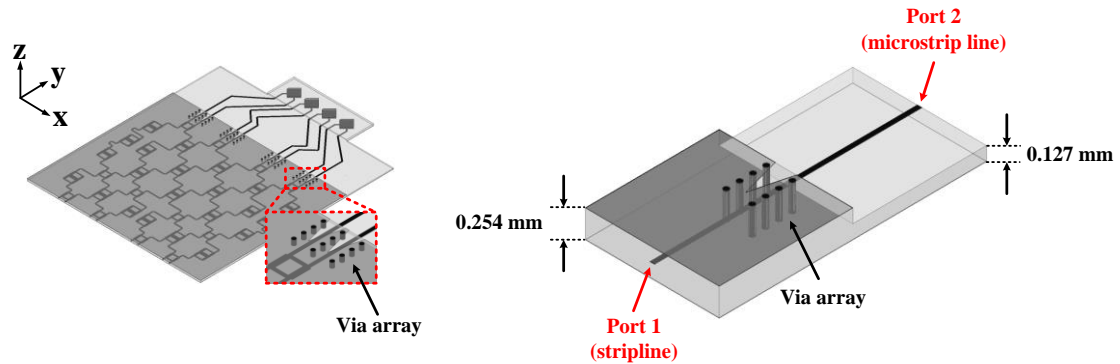


Figure 7. Structure of the transition part.

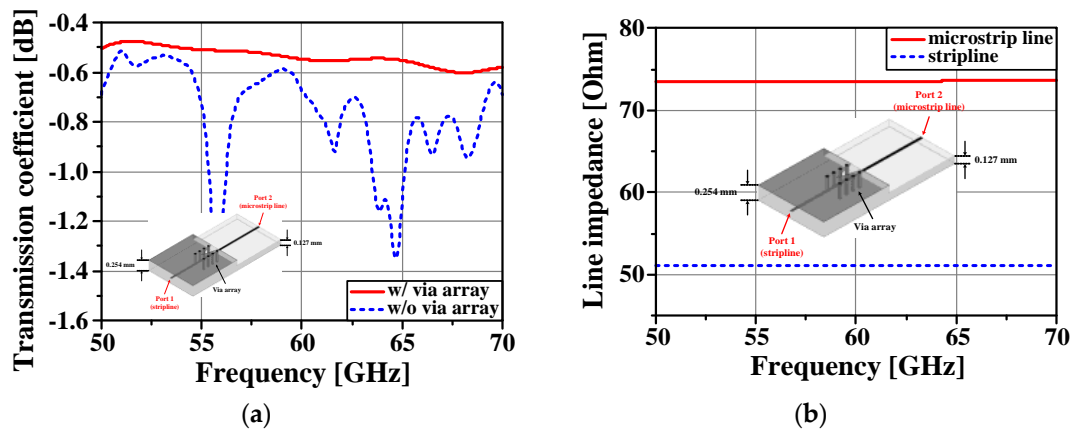


Figure 8. Simulated results of the transition part: (a) transmission coefficient with and without series via array and (b) line impedance.

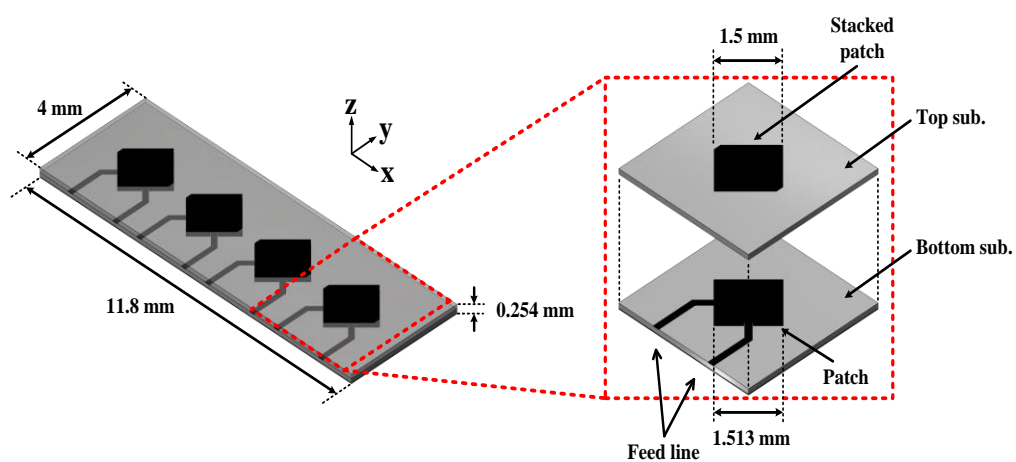


Figure 9. Geometry of the proposed  $1 \times 4$  patch array antenna.

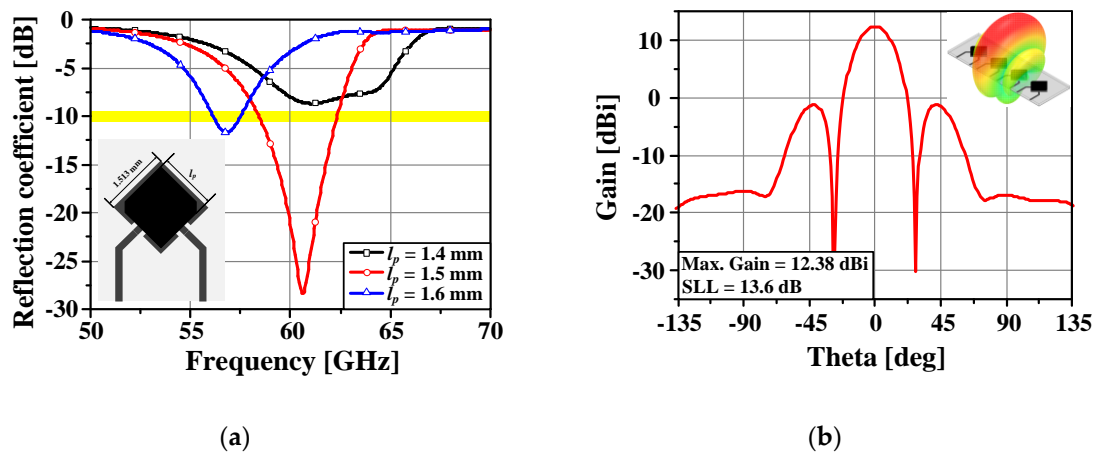


Figure 10. (a) Simulated reflection coefficient for various length of the parasitic stacked patch. (b) Simulated gain pattern of the patch antenna array.

### 3. Performance of the Proposed Antenna Array System

#### 3.1. Simulated Results

The simulated reflection coefficients of the proposed antenna array system with an  $8 \times 8$  Butler matrix are shown in Figure 11a. Over the frequency range of 55.3 GHz–64.9 GHz, the values of the reflection coefficients are lower than  $-10$  dB. Figure 11b shows the simulated mutual couplings between the input ports of the proposed antenna array system when port 4 is excited. The mutual couplings are less than  $-10$  dB over the frequency range of 57.5 GHz–63.2 GHz.

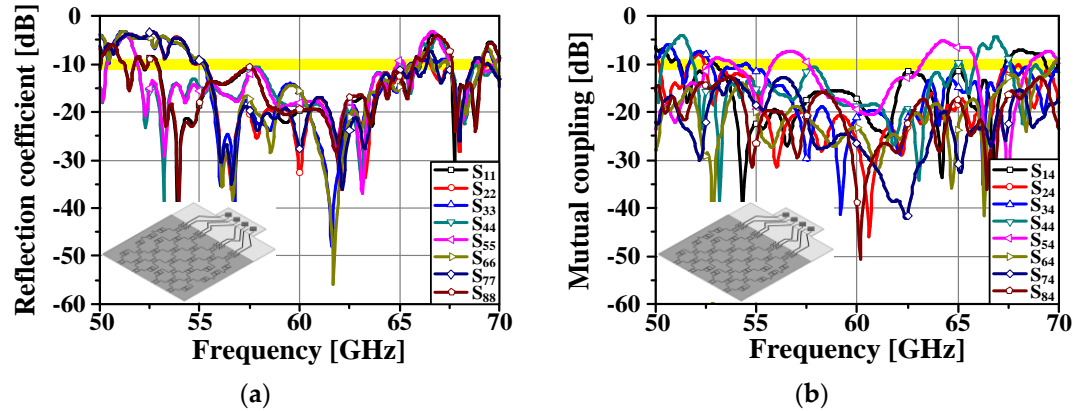


Figure 11. Simulated results of the proposed antenna array system: (a) reflection coefficient and (b) mutual coupling.

Figure 12 shows the simulated gain patterns in the  $xz$ -plane and the three-dimensional radiation patterns at 60 GHz of the proposed antenna array system when ports 2, 4, 5, and 7 are excited. At 60 GHz, the maximum gains are 9.39 dBi, 10.67 dBi, 10.63 dBi, and 9.38 dBi when the input ports 2, 4, 5, and 7 are excited, respectively. The beam-steering angles are  $-38^\circ$ ,  $-11^\circ$ ,  $+11^\circ$ , and  $+39^\circ$ , respectively. At 57 GHz, the maximum gains and beam-steering angles for ports 2, 4, 5, and 7 are 7.51 dBi at  $-44^\circ$ , 9.37 dBi at  $-14^\circ$ , 9.33 dBi at  $+14^\circ$ , and 7.45 dBi at  $+45^\circ$ , respectively. At 62 GHz, the maximum gains and beam-steering angles for ports 2, 4, 5, and 7 are 8.61 dBi at  $-37^\circ$ , 10.01 dBi at  $-11^\circ$ , 9.87 dBi at  $+11^\circ$ , and 8.53 dBi at  $+37^\circ$ , respectively.

Figure 13a shows the simulated surface current distributions of the patch antenna array. It can be seen that the circularly rotating surface currents are formed on the patch conductors by the  $\pm 90^\circ$  phase difference between two inputs of the designed dual-fed patch antenna. The RHCP is formed when

four ports from port 1 to port 4 are excited and LHCP is formed when four ports from port 5 to port 8 are excited. The simulated axial ratios of the proposed antenna array system for the excitation of ports 2, 4, 5, and 7 of the Butler matrix are shown in Figure 13b. The axial ratios are less than 3 dB over the frequency range of 54.9 GHz–61.5 GHz. The operating modes of the proposed antenna array system for selecting each input port are listed in Table 2.

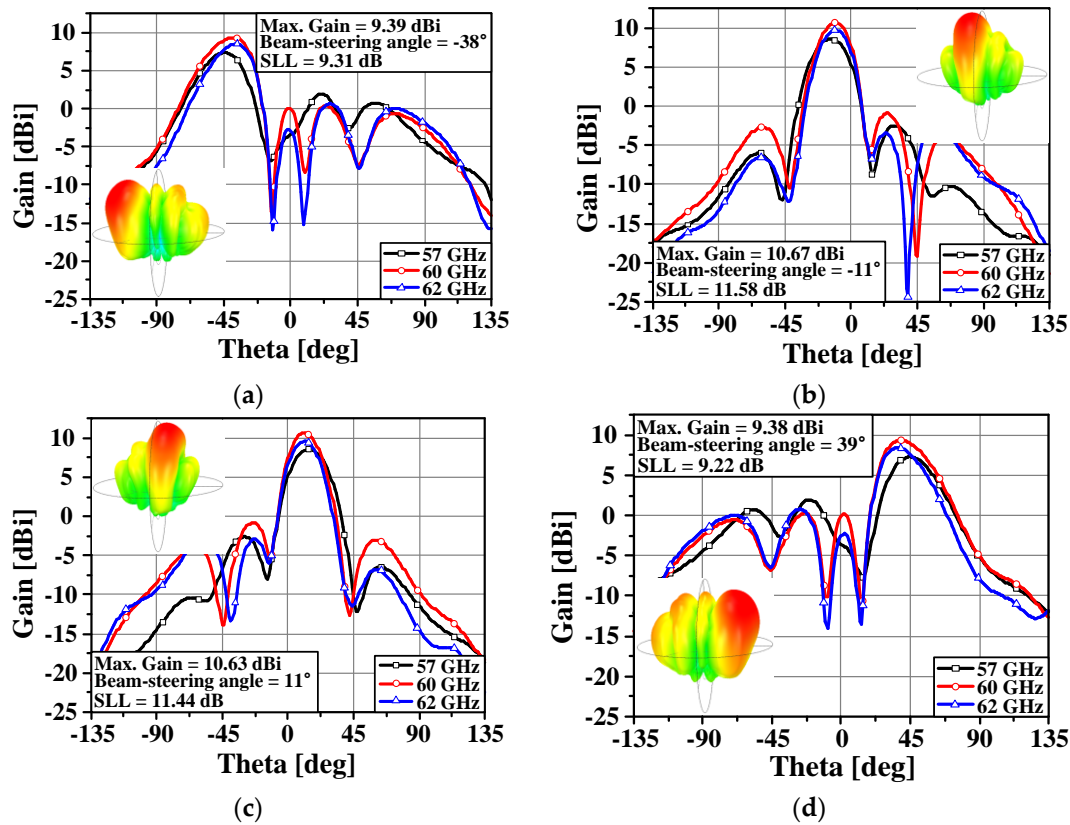


Figure 12. Simulated gain patterns of the proposed antenna array system with the excitation of (a) port 2, (b) port 4, (c) port 5, and (d) port 7.

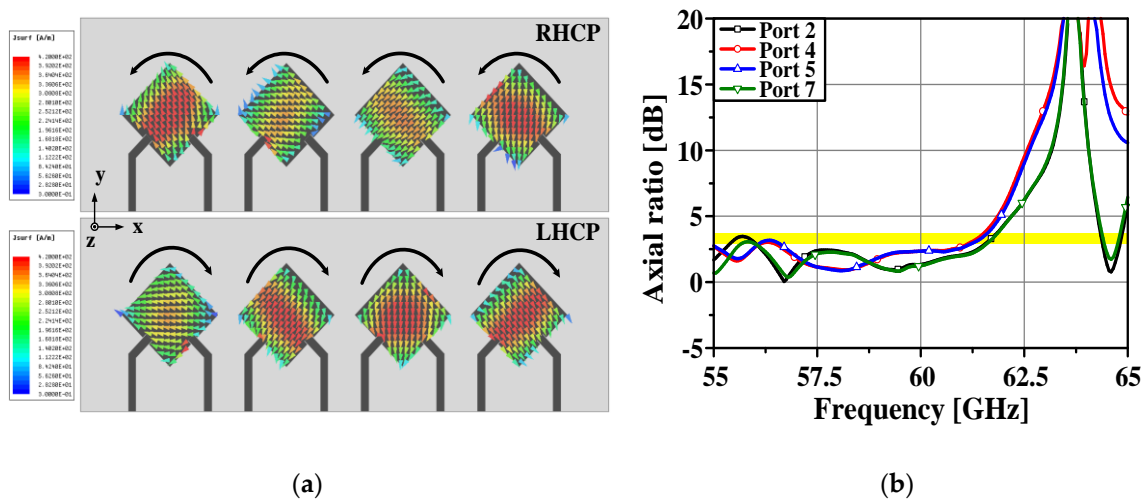


Figure 13. Simulated current distributions and the axial ratio: (a) surface current distributions of the patch antenna array and (b) axial ratio of the proposed antenna array system.

**Table 2.** Phases associated with the selected port of the  $8 \times 8$  Butler matrix.

Input Port	Beam-Steering Angle $\theta$ ( $xz$ -plane, $\phi = 0^\circ$ )	Polarization
Port 1	$+11^\circ$	RHCP
Port 2	$-38^\circ$	RHCP
Port 3	$+40^\circ$	RHCP
Port 4	$-11^\circ$	RHCP
Port 5	$+11^\circ$	LHCP
Port 6	$-39^\circ$	LHCP
Port 7	$+39^\circ$	LHCP
Port 8	$-11^\circ$	LHCP

### 3.2. Experimental Results

To account for the effect of using an actual connector on the antenna performances, a simulation including the connector was carried out using the Ansys HFSS [22] and CST Microwave Studio [23]. The connector model was based on the datasheet from Southwest for a 1.85 mm end-launch connector. Figure 14 shows the modified antenna array system with the connector model for when port 2 and port 4 of the proposed antenna are excited. The transition part was added to properly mount the connector to the antenna array system.

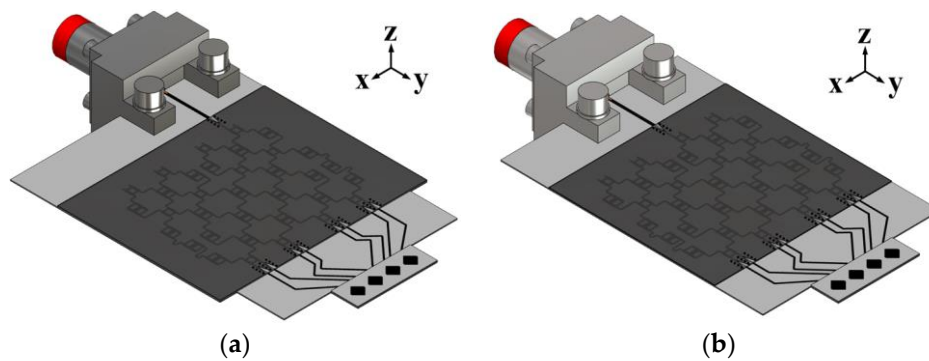
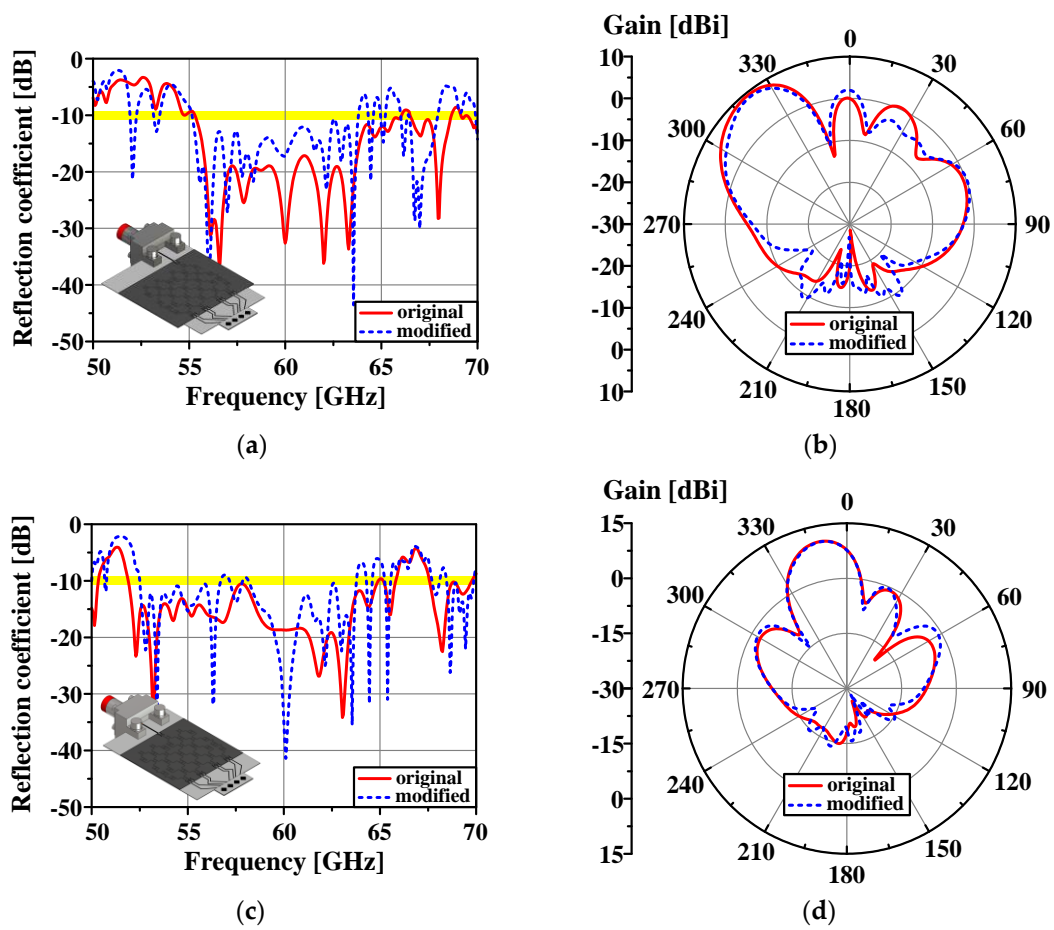


**Figure 14.** Modified connector model of the proposed antenna: (a) port 2 model and (b) port 4 model.

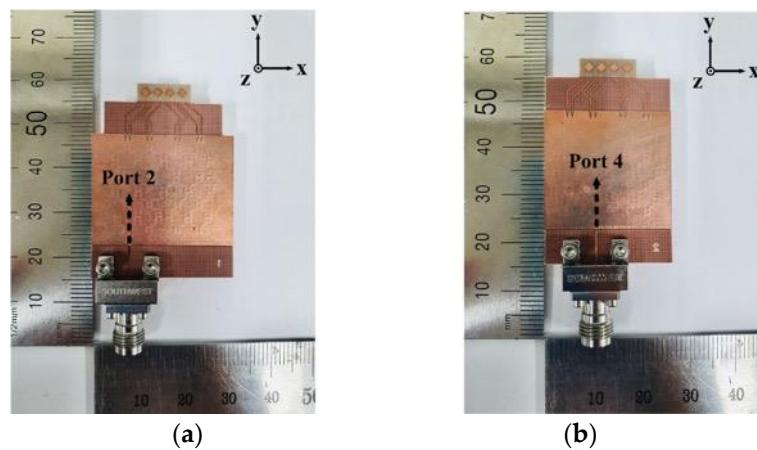
Figure 15 shows the comparison between the antenna array systems with and without the connector model on the reflection coefficient and the radiation pattern in the  $xz$ -plane. The simulated  $-10$  dB reflection coefficient bandwidths of the modified antenna array system with the connector model for port 2 and port 4 are 8.67 GHz (55.15 GHz–63.82 GHz) and 7.07 GHz (56.71 GHz–63.78 GHz), respectively. The radiation patterns of the modified antenna array system with the connector models agree well with those of the original antenna array system without the connector models.

Figure 16 shows the fabricated prototypes of the antenna with connector for port 2 and port 4. Figure 17 shows a photograph of the fabricated antenna and measurement setup. The fabricated antenna with a V-band connector is connected to a waveguide-to-coax adapter and a waveguide feed.

The simulated and measured reflection coefficients of the antenna are shown in Figure 18a,c. The measured  $-10$  dB  $S_{11}$  bandwidths of the antenna for port 2 model and port 4 model are 9.61 GHz (52.41 GHz–62.02 GHz) and 6.63 GHz (54.60 GHz–61.23 GHz), respectively. The simulated and measured normalized far-field radiation patterns at 60 GHz are shown in Figure 18b,d. For the port 2 model, the main beam points to the  $-35^\circ$  with a gain of 8.94 dBi. The direction of the main beam switches to  $-9^\circ$  with a gain of 10.18 dBi for the port 4 model. There is some discrepancy between the measured and simulated results, which is related to the fabrication tolerances realized in the alignment process and the effect of the glue for stacking the two substrates. Further, the output amplitude imbalance of the Butler matrix degrades the antenna gain.



**Figure 15.** Comparison of the simulated results between the original model and modified model: (a) reflection coefficient for port 2 model, (b) radiation pattern for port 2 model, (c) reflection coefficient for port 4 model, and (d) radiation pattern for port 4 model.



**Figure 16.** Fabricated prototypes of the antenna: (a) port 2 model and (b) port 4 model.

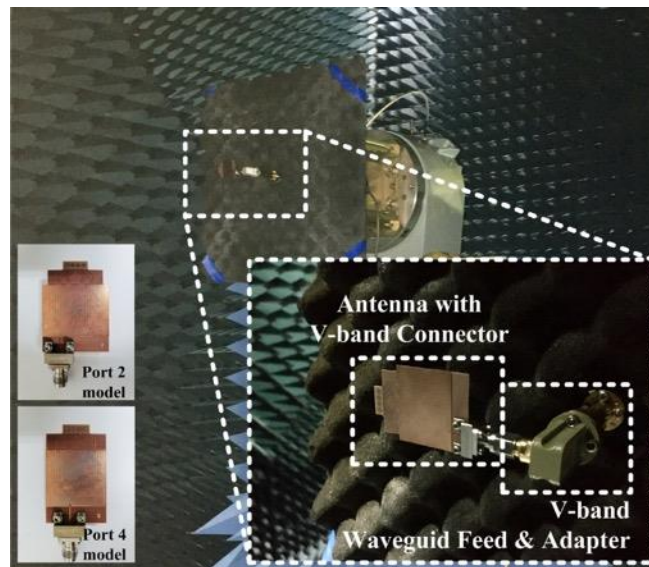


Figure 17. Fabricated antenna and measurement setup.

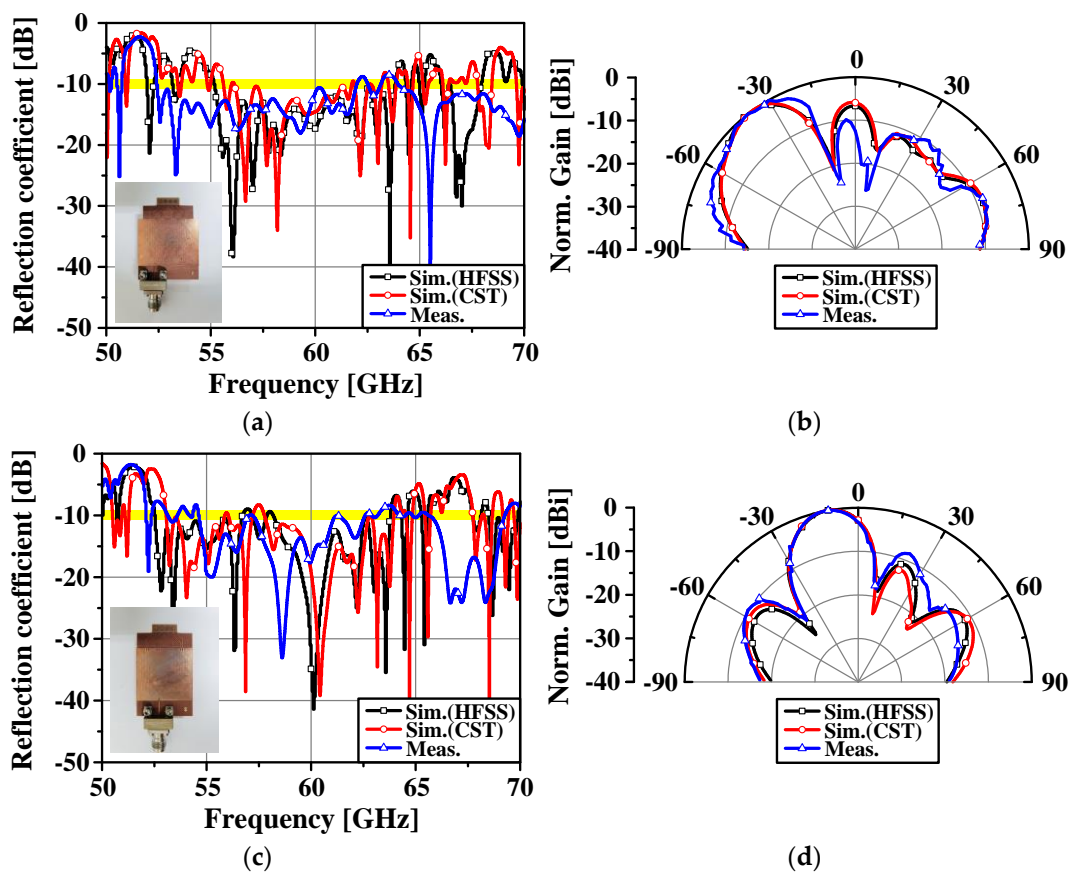
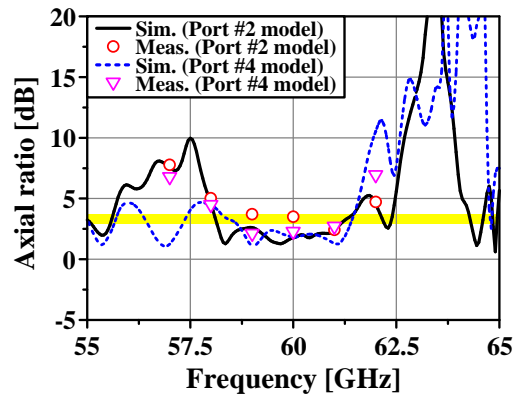


Figure 18. Measured results of reflection coefficient and radiation pattern: (a) reflection coefficient for port 2 model, (b) radiation pattern for port 2 model, (c) reflection coefficient for port 4 model, and (d) radiation pattern for port 4 model.

Figure 19 shows the measured axial ratio of the antenna for the port 2 model and port 4 model. Due to the losses induced by the connector and microstrip line-to-stripline transition part, the measured and simulated axial ratios differ slightly from the results of the original antenna array system without

the connector model. The values of the measured axial ratio for each port model agree reasonably well with the simulated ones, but the measured values are slightly worse than simulated ones, reflecting the real-world manufacturing tolerances.



**Figure 19.** Measured axial ratio of the antenna for port 2 model and port 4 model.

The comparison of various antenna array systems integrated with a Butler matrix is given in Table 3. Compared with previous works, it is proven that the proposed antenna array system demonstrates good beam-steering capability and polarization characteristics without a big difference in size and gain.

**Table 3.** Comparison of various antenna array systems integrated with a Butler matrix.

	[3]	[4]	[19]	This Work
Configuration	2 × 4 Patch (8 × 8 BM)	1 × 4 Patch (4 × 4 BM)	1 × 6 ME Dipole (5 × 6 BM)	1 × 4 Patch (8 × 8 BM)
Center Frequency [GHz]	60	60	28	60
10 dB Return Loss Bandwidth [GHz]	7	5.3	1	9.6
Dimensions [mm × mm × mm]	27 × 40 × 0.254 (5.4λ <sub>0</sub> × 8λ <sub>0</sub> × 0.05λ <sub>0</sub> )	9.75 × 13.1 × 0.127 (2λ <sub>0</sub> × 2.6λ <sub>0</sub> × 0.03λ <sub>0</sub> )	65 × 95 × 2.032 (6λ <sub>0</sub> × 8.8λ <sub>0</sub> × 0.19λ <sub>0</sub> )	25.7 × 32 × 0.254 (5.1λ <sub>0</sub> × 6.5λ <sub>0</sub> × 0.05λ <sub>0</sub> )
Peak Gain [dBi] sim./meas.	12.1/12.3	N/A/8.9	13.7/11.7	10.67/10.18
BM Insertion Loss [dB]	11	7.5	8.5	10.5
BM Phase Error [deg]	N/A	±10	±10	±29
Number of Scanning Beams	8 (2-D scanning)	4 (±14°/±40°)	5 (0°/±20°/±40°)	4 (±11°/±40°)
Polarization Diversity	No	No	No	Yes
Polarization Type	Linear	Linear	Circular	Dual-Circular

BM: Butler matrix.

#### 4. Conclusions

In this paper, a beam-steerable dual-circularly polarized 60 GHz patch antenna array is proposed. A 1 × 4 dual-fed stacked patch antenna array is integrated with an 8 × 8 Butler matrix. By utilizing the 8 × 8 Butler matrix, the proposed antenna array generates dual-circular polarization with a beam-steering capability. Depending on the excitation status of each input port of the 8 × 8 Butler matrix, the main beam of the antenna array can be steered in four directions and the polarization property (RHCP or LHCP) is determined. The reflection coefficient, beam-steering performance, and axial ratio of the antenna were analyzed at 60 GHz. The measured results for the fabricated antenna agreed well with the simulated ones. Thus, the proposed antenna array system could be a good candidate for millimeter-wave 5G applications that require wide beam coverage and polarization diversity.

**Author Contributions:** The presented work was carried out in collaboration between all the authors. Y.P. wrote the paper. J.B. participated in the conception. J.C. supervised the research. All authors have read and agreed to the published version of the manuscript.

**Funding:** This work was supported by Institute of Information & communications Technology Planning & Evaluation (IITP) grant funded by the Korea government(MSIT) (2018-0-00732, Fundamental research for solving the bottleneck technology of millimeter wave 5G cellular array antenna).

**Conflicts of Interest:** The authors declare no conflict of interest.

## References

1. Youngtaek, H.; Jaehoon, C. 60 GHz Patch Antenna Array With Parasitic Elements for Smart Glasses. *IEEE Antennas Wirel. Propag. Lett.* **2018**, *17*, 1252–1256.
2. Jihoon, B.; Jaehoon, C. A SAR Reduced mm-Wave Beam-Steerable Array Antenna With Dual-Mode Operation for Fully Metal-Covered 5G Cellular Handsets. *IEEE Antennas Wirel. Propag. Lett.* **2018**, *17*, 1118–1122.
3. Moulder, W.F.; Khalil, W.; Volakis, J.L. 60-GHz Two-Dimensionally Scanning Array Employing Wideband Planar Switched Beam Network. *IEEE Antennas Wirel. Propag. Lett.* **2010**, *9*, 818–821. [[CrossRef](#)]
4. Tseng, C.; Chen, C.; Chu, T. A Low-Cost 60-GHz Switched-Beam Patch Antenna Array With Butler Matrix Network. *IEEE Antennas Wirel. Propag. Lett.* **2008**, *7*, 432–435. [[CrossRef](#)]
5. Erfani, E.; Moldovan, E.; Tatu, S. A 60-GHz multi-beam antenna array design by using MHMICs technology. *Microw. Opt. Technol. Lett.* **2016**, *58*, 1844–1847. [[CrossRef](#)]
6. Trinh-Van, S.; Jongmin, L.; Youngoo, Y.; Kangyoon, L.; Keumcheol, H. A Sidelobe-Reduced, Four-Beam Array Antenna Fed by a Modified 4×4 Butler Matrix for 5G Applications. *IEEE Trans. Antennas Propag.* **2019**, *67*, 4528–4536. [[CrossRef](#)]
7. Tian, G.; Yang, J.; Wu, W. A Novel Compact Butler Matrix Without Phase Shifter. *IEEE Microw. Wirel. Compon. Lett.* **2014**, *24*, 306–308. [[CrossRef](#)]
8. Ren, H.; Arigong, B.; Zhou, M.; Ding, J.; Zhang, H. A Novel Design of 4×4 Butler Matrix With Relatively Flexible Phase Differences. *IEEE Antennas Wirel. Propag. Lett.* **2016**, *15*, 1277–1280. [[CrossRef](#)]
9. Zhai, Y.; Fang, X.; Ding, K.; He, F. Miniaturization Design for 8×8 Butler Matrix Based on Back-to-Back Bilayer Microstrip. *Int. J. Antennas Propag.* **2014**, *2014*. [[CrossRef](#)]
10. Adamidis, G.A.; Vardiambasis, I.O.; Ioannidou, M.P.; Kapetanakis, T.N. Design and Implementation of Single-Layer 4×4 and 8×8 Butler Matrices for Multibeam Antenna Arrays. *Int. J. Antennas Propag.* **2019**, *2019*. [[CrossRef](#)]
11. Krzysztof, W.; Slawomir, G. Broadband Integrated 8×8 Butler Matrix Utilizing Quadrature Couplers and Schiffman Phase Shifters for Multibeam Antennas With Broadside Beam. *IEEE Trans. Microw. Theory Tech.* **2016**, *64*, 2596–2604.
12. Chia-Chan, C.; Ruey-Hsuan, L.; Ting-Yen, S. Design of a Beam Switching/Steering Butler Matrix for Phased Array System. *IEEE Trans. Antennas Propag.* **2010**, *58*, 367–374. [[CrossRef](#)]
13. Gao, J.; Li, K.; Sato, T.; Harada, H. Novel dual polarized array antennas for 60 GHz mmWPAN applications. In Proceedings of the 2009 IEEE Antennas Propagation Society International Symposium, Charleston, SC, USA, 1–5 June 2009; pp. 1–4.
14. Rousstia, M.W.; Herben, M.H.A.J. High performance 60-GHz dielectric rod antenna with dual circular polarization. In Proceedings of the 2013 European Microwave Conference, Nuremberg, Germany, 9–11 October 2013; pp. 1671–1674.
15. Elkarkraoui, T.; Hakem, N.; Delisle, G.Y.; Coulibaly, Y. A Novel Design Approach for a 60 GHz Circularly Polarized EBG Antenna. *Prog. Electromagn. Res. C* **2016**, *69*, 37–51. [[CrossRef](#)]
16. Lamminen, A.; Aurinsalo, J.; Säily, J.; Karttaavi, T.; Francey, J.; Bateman, T. Dual-circular polarised patch antenna array on LCP for 60 GHz millimetre-wave identification. In Proceedings of the 8th European Conference on Antennas and Propagation (EuCAP 2014), Hague, The Netherlands, 6–11 April 2014; pp. 537–541.
17. Yao, Y.; Zhang, F.; Zhang, F. A New Approach to Design Circularly Polarized Beam-Steering Antenna Arrays Without Phase Shift Circuits. *IEEE Trans. Antennas Propag.* **2018**, *66*, 2354–2364. [[CrossRef](#)]
18. Li, Y.; Luk, K. A 60-GHz Wideband Circularly Polarized Aperture-Coupled Magneto-Electric Dipole Antenna Array. *IEEE Trans. Antennas Propag.* **2016**, *64*, 1325–1333. [[CrossRef](#)]

19. Gong, R.; Ban, Y.; Lian, J.; Liu, Y.; Nie, Z. Circularly Polarized Multibeam Antenna Array of ME Dipole Fed by 5×6 Butler Matrix. *IEEE Antennas Wirel. Propag. Lett.* **2019**, *18*, 712–716. [[CrossRef](#)]
20. Dyab, W.M.; Sakr, A.A.; Wu, K. Dually-Polarized Butler Matrix for Base Stations with Polarization Diversity. *IEEE Trans. Microw. Theory Tech.* **2018**, *66*, 5543–5553. [[CrossRef](#)]
21. Pozar, D.M. *Microwave Engineering*, 4th ed.; John Wiley & Sons, Inc.: Hoboken, NJ, USA, 2011; pp. 343–347.
22. Ansys Corporation. *Ansys HFSS, ver. 2017.2*; Ansys Corporation: Canonsburg, PA, USA, 2018.
23. CST. *CST Microwave Studio, ver. 2019*; CST: Darmstadt, Germany, 2019.



© 2020 by the authors. Licensee MDPI, Basel, Switzerland. This article is an open access article distributed under the terms and conditions of the Creative Commons Attribution (CC BY) license (<http://creativecommons.org/licenses/by/4.0/>).